

# Searching for Complex, Weak or Tangled Magnetic Fields in the Blue Supergiant Rigel

Shultz M.<sup>1,2</sup>, Wade G. A.<sup>2</sup>, Neiner C.<sup>3</sup>, Manset N.<sup>4</sup>, Petit V.<sup>2,5</sup>, Grunhut J.<sup>1,2</sup>, Guinan E.<sup>6</sup>, Hanes D.<sup>1</sup> and the MiMeS Collaboration

<sup>1</sup> Queen’s University, Canada

<sup>2</sup> Royal Military College, Canada

<sup>3</sup> Paris–Meudon Observatory

<sup>4</sup> CFHT Corporation

<sup>5</sup> West Chester University, USA

<sup>6</sup> Villanova University, USA

## Abstract.

Seventy–eight high–resolution Stokes  $V$ ,  $Q$  and  $U$  spectra of the B8 Iae supergiant Rigel were obtained with the ESPaDOnS instrument at the CFHT, and its clone NARVAL at the TBL in the context of the Magnetism in Massive Stars (MiMeS) Large Program, with the aim of scrutinizing this core–collapse supernova progenitor for direct evidence of weak and/or complex magnetic fields. In this paper we describe the reduction and analysis of the data, the constraints obtained on any magnetic field present in the stellar photosphere, and the variability of photospheric and wind lines.

**Key words:** stars: early type – stars: supergiants – stars: magnetic fields – stars: winds – spectropolarimetry

## 1 Introduction

Rigel: a blue supergiant, the closest and most readily studied Type II supernova progenitor, and a known  $\alpha$  Cygni variable. The subject of a global monitoring campaign known as the “Rigel–thon”, involving long–term spectroscopic monitoring, Microvariability and Oscillations in STars (MOST) space photometry, and spectropolarimetry.

Like most OB stars,  $\beta$  Ori A shows no signs of an easily detected magnetic field, however, its proximity makes it practical to ask: does the star possess a weak or complex field geometry, which might reveal itself within a high resolution data set? 78 circular and linear polarisation spectra were thus obtained in 2009 and 2010, and analysed as part of the MiMeS project.

## 2 Observations

Over an epoch from 09/2009 to 02/2010, 65 Stokes  $V$  (circular polarisation) and 13 Stokes  $Q$  and  $U$  (linear polarisation) spectra spanning  $\sim 370$ – $1000$  nm with a mean resolving power  $R \sim 65000$  at 500 nm were taken with the ESPaDOnS spectropolarimeter at the CFHT and its clone, NARVAL, at the TBL. Integration times were typically of a few–second duration. Acquisition of the spectropolarimetry and other ground–based campaigns occurred before, during and after the

Table 1: **Rigel at a Glance.** Observational and physical parameters of  $\beta$  Ori as derived from previous studies. Angular radius  $\theta_D$  is taken from Aufdenberg et al. (2008);  $v_\infty$  is from Bates et al. (1980);  $\dot{M}$  is from Barlow & Cohen (1977), Abbot (1980), and Puls et al. (2008); all other properties are derived in Przybilla et al. (2006).

spectral class	B8 Iae
Association	Ori OB 1
$V$	0.12
$M_V$	-7.84
$\log g$	$1.75 \pm 0.10$
$T_{\text{eff}}$	$12000 \pm 200$ K
Parallax	$4.22 \pm 0.11$ mas
$\theta_D$	$2.76 \pm 0.01$
$v_\infty$	400 – 600 km/s
$\dot{M}$	$10^{-7} - 10^{-6} M_\odot/\text{yr}$
$v \sin i$	$36 \pm 5$ km/s
distance	$240 \pm 50$ pc
radius	$70 \pm 14 R_\odot$

collection of the MOST data, with the period of densest sampling corresponding to the collection of MOST data.

### 3 Magnetic Analysis

Least Squares Deconvolution (LSD) was employed to extract high  $S/N$  ratio mean Stokes  $I$ ,  $V$ , and diagnostic  $N$  profiles from the circular polarisation spectra. The LSD line mask was cleaned to eliminate the contamination from telluric, emission and Balmer lines, remove weak or apparently absent lines, while  $\sim 90$  remaining lines were empirically adjusted to reflect actual line depths (however, see LPV section.) The typical  $S/N$  ratio in the Stokes  $V$  mean profiles was  $\sim 20\,000$ . No significant circular polarisation was detected in any of the 65 high precision Stokes  $V$  LSD profiles nor in any of the diagnostic  $N$  profiles.

Each LSD profile was then analysed to determine the longitudinal magnetic field  $B_l$  (Fig. 1). No significant longitudinal field was detected with a median  $1\sigma$  uncertainty in the individual measurements of 13 G. The distribution of  $B_l$  values inferred from the Stokes  $V$  is statistically identical to that, inferred from the diagnostic  $N$ . The measured longitudinal field was then compared to a grid of synthetic longitudinal field curves corresponding to the dipole magnetic fields with  $0^\circ \leq i \leq 90^\circ$ ,  $0^\circ \leq \beta \leq 90^\circ$ , and polar field strength  $B_d$  from 0 to  $\sim 3$  kG, where  $i$  is the angle of inclination from the line of sight and  $\beta$  is the magnetic obliquity. The radius of Rigel was determined from the interferometric angular radius (Aufdenberg et al., 2008) together with the distance calculated using the Hipparcos parallax (see Table 1). The inferred  $v \sin i$  (Przybilla et al., 2006) thus allows an upper bound on the rotational period of  $\sim 93$  d (corresponding to  $i = 90^\circ$ ), while the calculation of the breakup velocity ( $\sim 250$  km/s) provides a lower limit of  $\sim 13$  d. For ( $i = 90^\circ$ ,  $\beta = 90^\circ$ ) the maximum dipole field compatible with the data at  $3\sigma$  confidence is  $B_d \sim 20$  G, while  $B_d$  is constrained to be below  $\sim 50$  G for the intermediate values of  $i$  and  $\beta$  (see Fig. 2). Fields at this level, if present at the surface of Rigel, remain capable of strongly influencing the wind (ud-Doula & Owocki, 2002), yielding a wind magnetic confinement parameter  $\eta^* \sim 2 - 90$ , depending on the mass loss  $\dot{M}$  and the wind terminal velocity  $v_\infty$  values which remain poorly constrained.

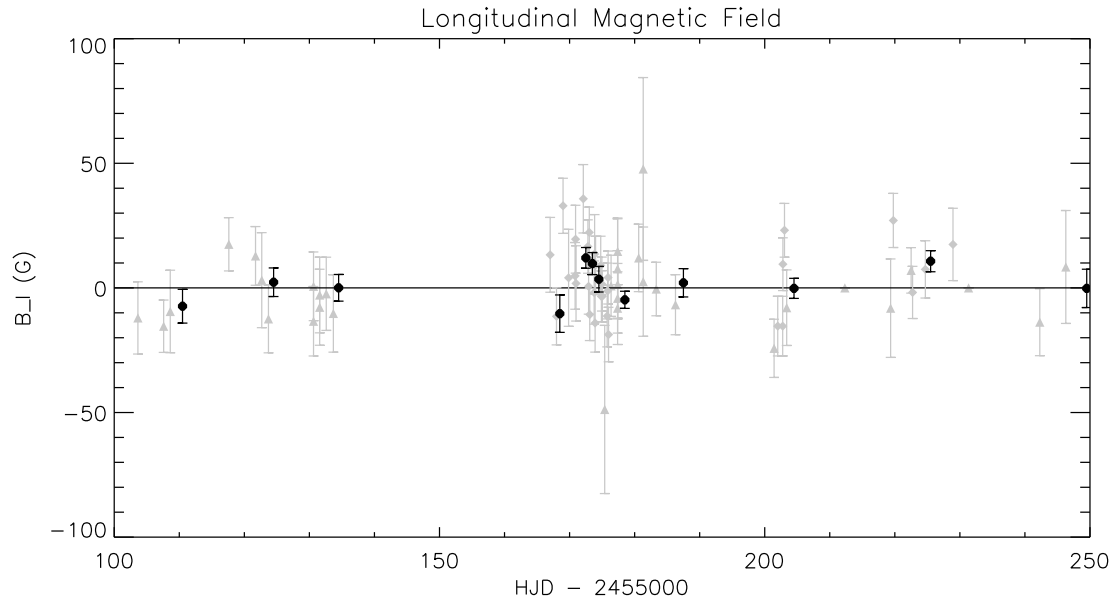


Figure 1: **Longitudinal Field Measurements.** Longitudinal field as calculated from Stokes  $V$  profiles as a function of HJD. Grey corresponds to single-observation calculations, with triangles denoting the NARVAL measurements, and diamonds marking the ESPaDOnS observations. Black points are calculated from weighted mean Stokes  $V$  profiles.

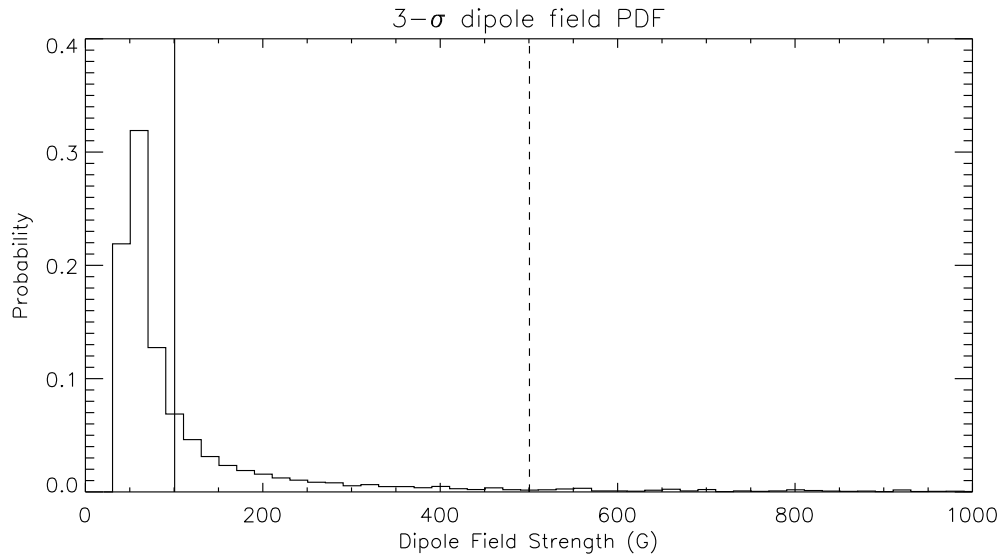


Figure 2: **PDF of  $\chi^2$  Landscape.** Histogram of the distribution of  $3\sigma$  upper limits to the dipolar field strength for all possible values of  $[i, \beta]$ . The solid line denotes the  $1\sigma$  confidence; the dashed line,  $2\sigma$  confidence. The  $3\sigma$  line is not shown, and appears at  $\sim 2800$  G.

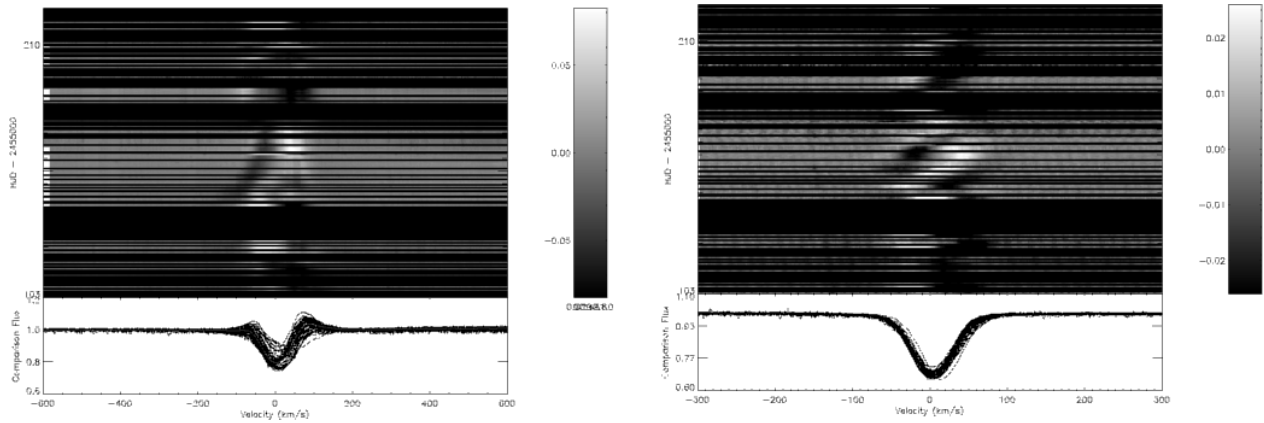


Figure 3: **Left:**  $H\alpha$  line. Note the HVA appearing at  $\sim -100$  km/s at the beginning of the most densely sampled epoch and evolving over a period of  $\sim 1$  month. The time axis is slightly asynchronous in order to display the data at maximum time-resolution. **Right:** Si II line at 637.1 nm. Note the apparent pulsational activity, coincident with the weak HVA.

## 4 Line Profile Variability

Rigel is a long-known  $\alpha$  Cygni variable (Sanford, 1947), with significant line profile variability (LPV) in  $H\alpha$  as well as various metal lines, which may be associated with any or all of the following factors (Kaufer et al., 1996b, 1997): mass loss events, photospheric spots, localized magnetic corotating interacting structures, rapid ionisation variations in a critical-state circumstellar environment, and/or  $g$ - or  $p$ -mode pulsations. Distinct LPV is seen in  $H\alpha$  as compared to metal lines (Fig. 3): the former with strong emission, variable over a broad velocity range and seemingly aperiodic (consistent with earlier spectroscopic monitoring (Kaufer et al., 1996a, 1996b; Israelian et al., 1997); the latter with a small apparent emission excess, and with variability, suggestive of periodic behaviour. Notable in the  $H\alpha$  line is a High Velocity Absorption event, albeit much weaker than those found in previous observations (Kaufer et al., 1997; Morrison et al., 2008). Amongst the most complexly variable metal lines is the O triplet at 777 nm; when these were removed from the line mask, numerous statistical ‘detections’ disappeared.

## 5 Conclusions, Future Work

No evidence of magnetic field is obtained in 65 high precision Stokes  $V$  observations of Rigel. Significant variability is observed in numerous spectral lines, with some suggestion of periodicity on the order of  $\sim 1$  month in metallic lines. Further modelling of Stokes  $V$  profiles using a disk-integrated model will be performed in order to obtain quantitative constraints on various potential field topologies, such as the subsurface metal opacity bump convection zone-driven dynamo-generated field proposed by Cantiello et al. (2009). In addition, a more detailed analysis of the line profile variability may allow characterisation of the circumstellar wind environment, which can then be compared to the predictions of the magnetically confined wind model (ud-Doula & Owocki, 2002).

**Acknowledgements.** We would like to thank James Silvester, who provided invaluable assistance in the construction of the line mask; the staff at the Canada–France–Hawaii Telescope and the Bernardot Lyot Telescope; and finally, the Natural Sciences and Engineering Research Council of Canada, whose funding allowed this work to proceed.

## References

- Abbot D. C., Biegging J. H., Churchwell E., Cassinelli J. P., 1980 *ApJ*, 238, 196
- Aufdenberg J. P., Ludwig H.-G., Kervella P., Mérand A., Ridgway S. T., Coudé du Foresto V., ten Brummelaar T. A., Berger D. H., Sturmman J., Turner N. H., 2008, in: *ESO Astrophysics Symposia*, “The Power of Optical/IR Interferometry: Recent Scientific Results and 2nd Generation Instrumentation”, Springer, 71
- Barlow M. J., Cohen M., 1977, *ApJ*, 213, 737
- Bates B., Giaretta D. L., McCartney D. J., McQuoid J. A., Bankhead R. E. L., 1980, *MNRAS*, 190, 611
- Cantiello M., Langer N., Brott I., de Koter A., Shore S. N., Vink J. S., Voegler A., Lennon D. J., Yoon S.-C., 2009, *A&A*, 499, 279
- Israelian G., Chentsov E., Musaev F., 1997 *MNRAS*, 290, 521
- Kaufer A., Stahl O., Wolf B., Fullerton A. W., Gaeng T., Gummertsbach C. A., Jankovics I., Kovacs J., Mandel H., Peitz J., Rivinius T., Szeifert T., 1997, *A&A*, 320, 273
- Kaufer A., Stahl O., Wolf B., Gaeng T., Gummertsbach C. A., Jankovics I., Kovacs J., Mandel H., Peitz J., Rivinius T., Szeifert T., 1996a, *A&A*, 314, 599
- Kaufer A., Stahl O., Wolf B., Gaeng T., Gummertsbach C. A., Kovacs J., Mandel H., Szeifert T., 1996b, *A&A*, 305, 887
- Morrison N., Rother S., Kurschat N., 2008 in: Hamann W.-R., Feldmeier A., Oskinova L. M. (eds), *Proc. Int. Workshop*, “Clumping in Hot-Star Winds”, 155
- Przybilla N., Butler K., Becker S. R., Kudritzki R. P., 2006, *A&A*, 445, 1099
- Puls J., Vink J. S., Najarro F., 2008, *Astron. Astroph. Rev.*, 16, 209
- Sanford R. F., 1947 *ApJ*, 105, 222
- ud-Doula A., Owocki S., 2002, *ApJ*, 576, 413